International Journal of Communication Systems

WILEY

RESEARCH ARTICLE OPEN ACCESS

The $\kappa - \mu$/Gamma-Rayleigh Fading Model: A Composite Fading Model for Powerline-Wireless Communication Channels

Kealeboga Mokise | Hermanus C. Myburgh

Department of Electrical, Electronic and Computer Engineering, University of Pretoria, Pretoria, Gauteng, South Africa

Correspondence: Kealeboga Mokise (kealeboga.mokise@up.ac.za)

Received: 8 February 2025 | **Revised:** 18 July 2025 | **Accepted:** 28 September 2025

Funding: The authors received no specific funding for this work.

Keywords: $\kappa - \mu$ fading | gamma-Rayleigh | multipath | PLC | shadowing

ABSTRACT

Statistical distributions are frequently used to model fading effects introduced by the communication channel on the received signal. Some distributions are directly derived from physical propagation models, while others are adapted from statistics and applied to model fading based on their goodness-of-fit to measurements or on account of their mathematical simplicity. In this paper, a line-of-sight (LOS) shadowed $\kappa - \mu$/gamma-Rayleigh ($\kappa - \mu$/GR) is proposed and thoroughly investigated. The GR distribution was selected for its mathematical simplicity and flexibility. Closed-form expressions for fundamental statistics such as the probability density function (PDF) and cumulative distribution function (CDF) are derived for the $\kappa - \mu$/GR fading model. Additionally, analytical expressions for higher-order moments, including the amount of fading (AF) and the moment generating function (MGF), are provided in closed-form expressions. Performance measures of interest, such as outage probability (OP), average symbol error probability (ASEP), and average channel capacity, are derived in closed-form for communication systems operating under the $\kappa - \mu$/GR channel fading conditions. The validity and utility of the proposed composite fading model for characterizing composite fading behavior observed in hybrid powerline-wireless communication (PLC-WLC) channels are demonstrated through an extensive series of theoretical comparisons with experimental PLC-WLC measurements. Hybrid PLC-WLC channel measurements were performed in various environments, and PLC-WLC propagation scenarios were classified according to the cable branching characteristics of the PLC segment of the hybrid PLC-WLC channel. The goodness-of-fit of the proposed composite fading model was evaluated using the Kullback-Leibler (KL) divergence test. The results revealed that the proposed composite fading model exhibited an excellent fit to the fading conditions encountered in hybrid PLC-WLC channels. Compared with other existing composite fading models, the $\kappa - \mu$/GR model provided the most accurate fitting results for measurements in large indoor environments, for which the propagation conditions present strong LOS signal components and weak scattered signal components. Furthermore, it was concluded on the basis of the obtained results that increased branching and terminations in the PLC channel of a PLC-WLC propagation environment lead to increased shadowing and multipath fading effects on the received signal and, consequently, to increased composite fading.

1 | Introduction

Signal fading is a well-recognized characteristic of radio wave propagation. Fading of the received signal is primarily attributed to two phenomena of signal propagation. The first, known as multipath propagation, occurs when a transmitted signal interacts with obstacles in the environment, such as buildings and terrain, leading to reflection, diffraction, and scattering. As a result, multiple signal components (MPCs) reach the receiver with varying delay times, amplitudes and phases, which causes fluctuations in signal strength around the signal strength mean value. The second phenomenon, signal shadowing, is attributed to obstructions between the transmitter and receiver devices, which lead to variations in the mean received signal strength due to changes in the propagation environment. This is particularly pronounced when there is relative movement between the communicating devices [1, 2]. The combined effect of multipath fading and shadowing results in composite fading, which provides a more comprehensive representation of signal strength variations and is essential for assessing the performance of radio communication systems.

Several composite fading models have been proposed to characterize the combined effects of multipath propagation and shadowing in various radio communication scenarios for various propagation environments. Composite fading models can be broadly classified into two categories. The first, known as shadowed line-of-sight (LOS), describes scenarios in which the dominant signal component is subject to shadowing. The second, referred to as multiplicative shadowed fading, accounts for shadowing of both the LOS component and the scattered signal components. Traditional composite fading models assume a Rayleigh or Nakagami-m distribution for the signal envelope in multiplicative shadowing cases, while the Rician distribution is often used in LOS shadowed models. In both cases, the shadowing component, which represents random fluctuations in the mean signal strength, is assumed to follow the lognormal [2, 3]. However, the lognormal distribution presents analytical challenges as it does not yield closed-form expressions of first-order and second-order statistics of interest.

To overcome the limitations associated with the lognormal distribution, alternative shadowing models such as the gamma distribution have been explored. The gamma distribution, known for its semi-heavy-tailed behavior, has facilitated the development of various composite fading models in the current literature. For instance, the authors in [4] proposed a Rayleigh/gamma composite fading model, also known as the K distribution, and the PDF expression of the model was obtained in closed-form. Additionally, it was shown that the gamma model excellently approximates the popular lognormal shadowing model. The generalized K distribution was introduced in [5], which is a Nakagami/gamma composite fading model, and the PDF expression of the model was obtained in closed-form. Additionally, the generalized K model was used to analyze communication systems using the differential phase shift keying (DPSK) modulation scheme under various fading conditions, and expressions for the performance metrics of interest, such as average BER and outage probability (OP), were obtained in closed-form. The inverse Gaussian distribution is another alternative shadowing model which has been proposed due to its excellent approximation to the lognormal distribution in heavy shadowing cases. In [6], the Rayleigh/inverse Gaussian composite fading model was proposed, and in [7], a generalized version, the Nakagami/inverse Gaussian, was proposed and several important tools for performance evaluation, such as the moment generating function (MGF), were derived in closed-form.

Generalized multipath fading models, such as $\kappa-\mu$ [8], $\eta-\mu$ [8], and $\alpha-\mu$ [9] have been proposed to describe the inherent complexity of the interaction between the propagating signal and the propagation environment. Subsequently, composite fading models based on the generalized fading models have been proposed. For example, the authors in [10] developed the $\kappa-\mu$/lognormal composite fading model. However, the PDF expression is subject to the evaluation of an infinite integral, and its computation requires the use of numerical methods. In other studies, the inverse Gaussian distribution was adopted for shadowing, leading to the development of the $\kappa-\mu$/inverse Gaussian and $\eta-\mu$/inverse Gaussian models in [11] and [12], respectively, and it was shown in both cases that the models obtain closed-form PDF expressions for specific parameter values. Furthermore, the gamma distribution has been used to develop models such as the $\kappa-\mu$/gamma [13, 14] and $\eta-\mu$/gamma [15, 16], and in both cases, the expressions of the PDFs were obtained in terms of an infinite series representation, and closed-form expressions were obtained for specific cases of associated parameters. Recent studies have also explored the use of inverse gamma distribution [17] and Nakagami-m as shadowing models [18] to enhance the tractability of composite fading models. In [19], the authors conduct an in-depth investigation of the utility of the inverse gamma distribution to characterize shadowing. A comparison of the inverse gamma model with published results shows that it is an excellent model to describe shadow fading in real-world measurements. The authors in [20] conduct a detailed investigation of single shadowed and double shadowed composite fading models by assuming the $\kappa-\mu$ multipath model and either a Nakagami-m or inverse Nakagami-m shadowing model. It is evident from the preceding research that signal propagation in composite fading environments is very complex. Due to this inherent complexity, distributions that are sometimes derived purely as mathematical or statistical solutions can be borrowed and applied to describe a physical signal propagation phenomenon on account of their goodness-of-fit to communications channel measurements or their mathematical tractability. Notably, distributions such as Weibull [21] and Lomax [22], log-logistic (also known as the Fisk distribution) [23] have been applied in such contexts.

In the current literature, composite fading has been intensively studied and validated in wireless communication (WLC) scenarios. The powerline communication (PLC) channel is a known medium of radio signal propagation, and it exhibits propagation characteristics which are apparent in wireless channels, such as multipath propagation and signal propagation path-loss. A hybrid PLC-WLC communication channel can be established by allowing the transmitter device to inject a high-frequency signal into a PLC channel, which will be radiated through the unshielded powerline cables, and will be received wirelessly by the receiver with an antenna element connected to it. However, such unwanted radiation of high-frequency communication signals is an unattractive

phenomenon of PLC channels, and it has always been challenging to deal with it. Moreover, it is considered to be a hindrance to the widespread adoption of PLC systems. Among several attempts to tackle this challenge, the authors in [24] present an empirical method to characterize the radiation patterns of several types of powerline cables, and it is shown that the radiation patterns deviate from the theory due to current variability of PLC channels. Moreover, the outdoor PLC environment exhibits higher attenuation and less variation of radiation levels compared to the indoor PLC environment [25]. In [26], a signal processing technique for channel impulse response (CIR) measurements of indoor PLC channels is presented, and it is shown that unwanted radiation could be reduced by 10 dB. The authors in [27] present a bottom-up PLC channel model that takes into account unwanted radiation modelled as resistance elements, and comparisons of the derived model with measurements showed an excellent fit. In contrast, a number of studies have taken a different approach to exploit the unwanted radiation of PLC channels. In [28], a wideband frequency channel sounding method was used to characterize the PLC-to-WLC propagation path and the WLC-to-PLC propagation path. The frequency response in both directions was comparable in signal strength, meaning that the magnitude response is independent of the signal propagation direction, which led to the conclusion that such a hybrid channel is symmetrical. In [29], channel frequency response (CFR) magnitudes obtained from a measurement campaign were fitted to various statistical distributions, and based on the criteria of the relative frequency associated with the chosen statistical distribution for all CFR measurements, the lognormal distribution was chosen as the best-fit. The authors in [30] present the characterization of a hybrid PLC-WLC channel in the 2.4-GHz ISM frequency band, in which the PLC channel is used as an antenna to receive the signal from a wireless modem. The results show that, in terms of data transfer rates, a PLC-WLC channel outperforms the WLC channel in the 2.4-GHz band in non-line-of-sight (NLOS) propagation scenarios.

Immobility is one of the hindrances, among others, which slow down the mass adoption of PLC technology because end-nodes are physically connected to the powerline cables. A PLC-WLC communication channel is a solution to this dilemma because it allows the end-nodes to be mobile and physically separated from the dangerous high-voltage live PLC channel. Previous works on hybrid PLC-WLC channel characterization primarily focus on the frequency-selective behavior of such a channel, and PLC-WLC propagation environments are typically investigated with both the transmitter and receiver remaining stationary during channel measurements. Therefore, in the current literature, there is a significant lack of time-selective behavior characterization, and characterization of hybrid PLC-WLC propagation scenarios involving relative motion between the PLC and WLC devices. In a previous study [31], the authors presented the characterization of composite fading in hybrid PLC-WLC channels involving relative motion between the PLC and WLC devices. The received composite faded signal was separated into short-term (multipath) and long-term (shadowing) fading signal components, and various existing multipath and shadowing models were fitted to the measurements. It was found that the gamma and Nakagami-m distributions obtained the best-fit to long-term and short-term fading components, respectively, thereby demonstrating composite fading behavior. Moreover, it was found that PLC-WLC propagation scenarios with PLC channels having increased branches and terminations exhibit increased composite fading behavior.

Motivated by the above considerations and inspired by previous works in the literature, the present contribution extends the work done in [31] and investigates the composite fading phenomenon in mobile PLC-WLC propagation scenarios. Subsequently, the $\kappa-\mu$/gamma-Rayleigh (GR) composite fading model is proposed, whereby shadowing is assumed to be GR distributed. The GR distribution is borrowed from statistics, and it can be observed to exhibit an explicit semi-heavy-tailed behavior, which makes it suitable for modelling shadow fading behavior. Moreover, its analytical simplicity renders it an attractive alternative for describing shadowing. The shadowing severity behavior of the GR model is described by its derived amount-of-fading (AF). Furthermore, novel insights into the formulation of the composite fading problem in hybrid PLC-WLC channels are provided, as well as fundamental statistics and empirical validation of the $\kappa-\mu$/GR fading model. Accordingly, the main contributions of this paper can be summarized as follows:

- A problem formulation of time-selective behavior in PLC-WLC propagation environments is provided, thereby providing novel insights into the composite fading behavior in such PLC-WLC propagation environments.
- Derivation of the $\kappa-\mu$/GR fading model PDF expression in closed-form. Additional key statistical metrics such as the moment-generating function (MGF), cumulative distribution function (CDF), amount-of-fading (AF) and higher-order moments for the model are derived in closed-form.
- Analytical derivation of performance metrics such as average channel capacity, average symbol error probability (ASEP) and OP for communication systems operating in $\kappa-\mu$/GR fading conditions.
- Demonstration of the $\kappa-\mu$/GR fading model versatility by showing its special cases based on its associated parameters. The ability of the GR model to approximate other lognormal and inverse Gaussian composite fading models is demonstrated through novel closed-form parameter approximating expressions derived through method-of-moments (MoM) estimators.
- Empirical validation of the $\kappa-\mu$/GR fading model through extensive measurement campaigns in real-world indoor PLC-WLC propagation scenarios.

The remainder of the paper is organized as follows. Section 2 provides the problem formulation of composite fading behavior in PLC-WLC propagation environments. Section 3 introduces the proposed $\kappa-\mu$/GR composite fading model and provides details of the derivation of its fundamental statistics. In Section 4, special cases and approximations of other composite fading models are presented, which are deduced from the proposed model. Section 5 is devoted to the derivation of the performance metrics of interest, and in Section 6 the impact of the various parameters of the $\kappa-\mu$/GR fading channel on these metrics is examined. Section 7 outlines the experimental methods and signal propagation scenarios employed

to obtain real-world hybrid PLC-WLC channel measurements. The utility and validity of the proposed composite fading models are then evaluated and compared with existing models in Section 8. Finally, Section 9 provides some concluding remarks.

2 | Problem Formulation

The shared propagation characteristics of the PLC and WLC channels enable the transmission of radio signals between the two channels with minimal coupling requirements. However, signal coupling inevitably causes imbalances in the communication system, and this is primarily due to the asymmetry in signal conductors, electronic components and loads. This imbalance is the main factor leading to the conversion between differential-mode (DM) and common-mode (CM) currents [27]. A PLC modem connected to a powerline network will experience mode conversions since there is little control over the wiring infrastructure and the loads connected to the powerline. Although the load impedances of the integrated circuit (IC) components within powerline modems (PLMs) are optimized to reduce mode conversions, the inherent tolerances in the design and manufacturing processes still allow for these conversions. As a result, mode conversion can be categorized into two main types. The first type is mode conversion between the PLM and the coupling circuit, and the second type is mode conversion along the powerline propagation paths.

Unwanted CM transmission in a PLM is mainly caused by asymmetries in the conductors of the analog front-end IC, arising from trace grounding imbalances or the finite impedance connections between different ground planes [32]. While modern design and manufacturing techniques aim to generate nearly perfect DM signals, connecting a PLM to a long powerline cable induces DM-to-CM conversion due to parasitic coupling between the PLM and the powerline. The DM current generated by the PLM analog front-end produces magnetic fields that can couple with unshielded copper cables, creating a CM voltage. In addition, DM voltage signals from the PLM analog front-end can lead to CM currents on the powerline through capacitive coupling [33].

Mode conversion along the powerline propagation paths occurs because of localized variations in the electrical properties of the cables. These variations are caused by branches in the powerline network (PLN) where cables of different dielectric material thickness, copper conductor radius and length are joined together. Furthermore, cable bends and loops can disrupt the symmetry of the PLN, contributing to these variations. In indoor PLN settings, the presence of different loads connected to various termination points can further contribute to network asymmetry due to impedance mismatches between the loads. Additionally, the ground in indoor PLN environments exhibits finite resistance at high frequencies, which can induce imbalances between the loads and the ground. When such an imbalance exists, part of the DM signal can propagate along the CM path between the cable and ground at the termination point, resulting in a reduction in the power available to the load and generating CM currents. Moreover, the same imbalance at the termination can lead to CM-to-DM conversion, which may distort the transmitted DM signal received through the PLN [27].

Figure 1 illustrates a PLC-WLC channel, where the top half of the figure shows the PLC portion of the channel on the side view of a wall, and the bottom half shows the top view of the propagation environment. The points labelled *A*, *B*, *C*, *D*, and *E* are designated as instances of DM-to-CM mode conversion along the PLC channel. In a PLC communication system, the injected DM signal at *A* is intended to travel from the transmitter to the receiver through the conducting cables. However, mode conversion instances along the PLN result in unintended signal radiation emissions through the unshielded conducting cables. These unintended radiation emissions are leveraged in the PLC-WLC channel. In the illustrated scenario in Figure 1, the PLC-WLC communication system consists of a PLC transmitter and a mobile WLC receiver in the propagation environment, the receiver will intercept the radiated signal as it travels along the PLC channel path from point *A* to point *E*.

In WLC systems, a LOS path denotes a path that allows the radiated signal to propagate from the transmitter to the receiver with no obstruction and be received at maximum signal strength. Unlike in WLC systems, in the PLC-WLC system there is no direct signal path between the PLC transmitter and WLC receiver, but instead the powerline channel acts as an antenna element, thereby allowing the propagating signal to be radiated at various locations along the powerline and be received at various signal strengths in the wireless channel. An emitted signal from any of the various DM-to-CM mode conversion instances may be received through a LOS path, which denotes the path that allows the signal emitted from a mode conversion instance in the powerline channel to be received directly in the wireless channel without obstruction. Some of the emitted signals may undergo scattering in the wireless channel and the scattered components are received through NLOS paths, whereby a NLOS path denotes the path created when an emitted signal is reflected or diffracted by a scatterer in the wireless channel. The various LOS and NLOS paths are shown in Figure 1. The strongest signal emissions are shown to exist at point *A* and the weakest signal emissions exist at point *E*. The constructive or destructive interference

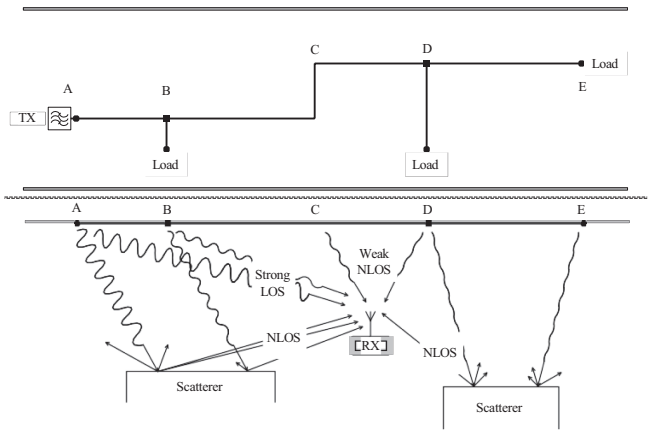

FIGURE 1 | Illustration of composite fading behavior in a hybrid PLC-WLC channel.

of the emitted signals results in random fluctuations of the received signal as the receiver moves or changes its location along the path of the PLC channel. A signal emitted from a DM-to-CM mode conversion instance that is received through a LOS path contributes to random fluctuations of the mean signal strength, leading to long-term variations (shadowing fading). Additionally, scattered signal components received through NLOS paths end up causing instantaneous variability in signal strength near the receiver, resulting in short-term variations (multipath fading). Given this concurrent behavior of long-term and short-term signal strength variability, it can be concluded that a signal propagating in such a PLC-WLC channel will experience composite fading.

3 | The $\kappa-\mu$/Gamma-Rayleigh Composite Fading Model

This section presents the proposed LOS shadowed composite fading model. Multipath fading is assumed to follow a $\kappa-\mu$ distribution, and shadow fading is assumed to follow a Gamma-Rayleigh (GR) distribution. The derivation of the composite fading model, and subsequent fundamental statistics, is inspired by the pioneering works of Paris [34] and Cotton [18].

3.1 | LOS Shadowing Signal Model

The propagation conditions in the $\kappa-\mu$/GR composite fading channel produce a received signal that is composed of clusters of multipath components, whereby each multipath cluster consists of a number of scattered multipath components and a dominant component. The scattered components exhibit random phases and nearly identical delay times, while the delay spreads between clusters are considerably larger [8]. Within each cluster, the scattered components are assumed to have equal power, whereas the power of the dominant component is assumed to be arbitrary and subject to random fluctuations due to shadowing [18]. Consequently, the envelope of the composite faded received signal, R, is expressed in terms of its in-phase and quadrature components as

$$R=\sqrt{\sum_{i=1}^{\mu}\left(X_i+\zeta p_i\right)^2+\left(Y_i+\zeta q_i\right)^2}, \tag{1}$$

in which μ denotes the number of multipath clusters. X_i and Y_i are mutually independent Gaussian random processes with zero mean, that is $\mathbb{E}[X_i]=\mathbb{E}[X_i]=0$, and variance $\mathbb{E}[X_i^2]=\mathbb{E}[X_i^2]=\sigma^2$. The parameters p_i and q_i represent the mean values of the in-phase and quadrature components for the ith cluster, while ζ denotes the random variable which is responsible for shadowing and is assumed to follow a GR distribution with parameters θ and α.

3.2 | The $\kappa-\mu$ Distribution

The $\kappa-\mu$ distribution is a fading model that describes the impact of multipath fading effects on the received signal under LOS signal propagating conditions. The versatility of the $\kappa-\mu$ distribution is attributed to its two distinct physical parameters, namely κ and μ. The μ parameter describes the multipath component clustering behavior of the propagation environment, and the parameter κ describes the power disparity between the dominant component and scattered components, which is given by the ratio of the dominant component power to the total power of the scattered components. The corresponding $\kappa-\mu$ fading model PDF for a received signal with envelope R and $\hat{r}=\sqrt{E[R^2]}$ is given by [8]

$$\begin{aligned} f_R(r)=&\frac{2\mu(\kappa+1)^{\frac{\mu+1}{2}}}{\kappa^{\frac{\mu-1}{2}}\exp(\kappa\mu)}\left(\frac{r}{\hat{r}}\right)^{\mu}\exp\left(-\mu(\kappa+1)\left(\frac{r}{\hat{r}}\right)^2\right)\\ &\times I_{\mu-1}\left[2\mu\sqrt{\kappa(\kappa+1)}\frac{r}{\hat{r}}\right], \end{aligned} \tag{2}$$

in which $\hat{r}$ is the root-mean-square value (rms) of R, $I_v(\cdot)$ is the modified Bessel function of the first kind of order v, the parameter $\kappa>0$ is the relationship between the total power of the dominant component (d^2) and the total power of the scattered components ($2\mu\sigma^2$), and $\mu>0$ is given as $\mu=\frac{E^2(R^2)}{Var(R^2)}\cdot\frac{1+2\kappa}{(1+\kappa)^2}$. Letting $d=\sqrt{2\mu\sigma^2\kappa}$ and $\sigma=\sqrt{\frac{\hat{r}^2}{2\mu(\kappa+1)}}$, (2) can be rewritten in a more compact form given by

$$f_R(r)=\frac{r^{\mu}}{\sigma^2 d^{\mu-1}}\exp\left(\frac{-r^2-d^2}{2\sigma^2}\right)I_{\mu-1}\left[\frac{dr}{\sigma^2}\right]. \tag{3}$$

3.3 | The Gamma-Rayleigh Distribution

The Gamma-Rayleigh (GR) model is a statistical distribution that arises from the Transformed-Transformer method, which is used to generate new families of continuous distributions. In the Transformed-Transformer method (also known as the $Y-V$ family), a random variable Y is transformed by another random variable V (referred to as the transformer) into a new random variable Z [35]. One particular $Y-V$ family introduced in [35] is the Gamma-V family, whereby Y follows the gamma distribution with parameters $\beta>0$ and $\alpha>0$, and its PDF is given by

$$f_Y(y)=\frac{\beta^{\alpha}}{\Gamma(\alpha)}y^{\alpha-1}\exp(-\beta y). \tag{4}$$

The GR distribution was introduced in [36], where V is a Rayleigh distributed random variable with a parameter $\sigma_v>0$ and a PDF given by

$$f_V(v)=\frac{v}{{\sigma_v}^2}\exp\left(-\frac{v^2}{2{\sigma_v}^2}\right). \tag{5}$$

According to [36], the new random variable Z is GR distributed with the PDF given by

$$f_Z(z)=\frac{2\theta^{\alpha}}{\Gamma(\alpha)}z^{2\alpha-1}\exp\left(-\theta z^2\right), \tag{6}$$

with the shape parameter $\alpha>0$ and scale parameter $\theta={}^{\beta}/_{2{\sigma_v}^2}$. The gamma and Rayleigh distributions are special cases of the GR distribution. Letting $w=z^2$, the power PDF is given by

$$f_W(w) = \frac{\theta^\alpha}{\Gamma(\alpha)} w^{2\alpha-1} \exp(-\theta w). \tag{7}$$

Using (7), the moments of the GR distribution are given by

$$E\left[W^k\right] = \frac{\Gamma(\alpha+k)}{\Gamma(\alpha)\theta^k}. \tag{8}$$

The amount of fading (AF) is a key performance metric in communication systems which quantifies the severity of fading. The AF is defined as

$$\mathrm{AF} = \frac{E\left[W^2\right]}{(E[W])^2} - 1. \tag{9}$$

For the GR distribution, the corresponding first-order ($k = 1$) and second-order ($k = 2$) moments can be computed via (8) and substituted into (9), which yields the closed-form expression

$$\mathrm{AF} = \frac{1}{\alpha}. \tag{10}$$

The AF expression given by (10) reveals that the physical interpretation of the GR distribution α parameter is the amount of shadowing and it inversely reflects the severity of shadowing. α parameter can take any value in the range $\alpha \geq 0$, therefore shadowing is most severe for $\alpha \to 0$, which corresponds to complete shadowing of the dominant signal component, and $\alpha \to \infty$ corresponds to no shadowing. It should be noted that in practice the extreme cases of $\alpha \to 0$ and $\alpha \to \infty$ are not met, which means some shadowing of the dominant signal component can always be expected.

3.4 | The $\kappa-\mu$/Gamma-Rayleigh Composite Distribution

The PDF of the received signal envelope, R, in a $\kappa-\mu$/GR composite fading channel can be determined by averaging the infinite integral of the conditional PDF of the $\kappa-\mu$ fading model with respect to the random variation of the mean signal power, Z, as follows

$$f_R = \int_0^\infty f_{R|Z}(r|z) f_Z(z) dz. \tag{11}$$

Using the compact form of the $\kappa-\mu$ distribution in (3), the conditional PDF $f_{R|Z}(r|z)$ is given by

$$f_{R|Z}(r|z) = \frac{r^\mu}{\sigma^2 (zd)^{\mu-1}} \exp\left(\frac{-r^2-(zd)^2}{2\sigma^2}\right) I_{\mu-1}\left(\frac{zdr}{\sigma^2}\right), \tag{12}$$

where the random variable Z follows the GR distribution given by (6). Substituting (6) and (12) into (11), the PDF of the proposed $\kappa-\mu/$ GR composite fading model can be expressed as follows:

$$\begin{aligned} f_R(r) = {} & \frac{2\theta^\alpha r^\mu \exp\left(-\frac{r^\mu}{2\sigma^2}\right)}{\sigma^2 d^{\mu-1}\Gamma(\alpha)} \int_0^\infty z^{2\alpha-\mu} \\ & \times \exp\left(-\left(\frac{d^2}{2\sigma^2}+\theta\right) z^2\right) I_{\mu-1}\left(\frac{zdr}{\sigma^2}\right) dz. \end{aligned} \tag{13}$$

The preceding integral can be solved using [37, eq. (2.15.5.4)], and along with some algebraic manipulation, and substituting $d = \sqrt{2\mu\sigma^2\kappa}$ and $\sigma = \sqrt{\frac{\hat{r}^2}{2\mu(\kappa+1)}}$, the resultant closed-from PDF expression of the $\kappa-\mu/$ GR distribution is given by

$$\begin{aligned} f_R(r) = {} & \frac{2\theta^\alpha \mu^\mu r^{2\mu-1}(\kappa+1)^\mu}{(\mu\kappa+\theta)^\alpha \Gamma(\mu)\hat{r}^{2\mu}} \exp\left(-\mu(\kappa+1)\frac{r^2}{\hat{r}^2}\right) \\ & \times {}_1F_1\left(\alpha;\mu;\frac{\mu^2\kappa(\kappa+1)r^2}{(\mu\kappa+\theta)\hat{r}^2}\right), \end{aligned} \tag{14}$$

in which ${}_1F_1(\cdot;\cdot;\cdot)$ denotes the confluent hypergeometric function. Now letting γ represent the instantaneous signal-to-noise ratio (SNR), and performing transformation of variables, $r = \sqrt{\gamma\hat{r}^2/\overline{\gamma}}$, on the envelope PDF given in (14), the corresponding SNR PDF $f_\gamma(\gamma)$ is given by

$$\begin{aligned} f_\gamma(\gamma) = {} & \frac{\theta^\alpha \mu^\mu \gamma^{\mu-1}(\kappa+1)^\mu}{(\mu\kappa+\theta)^\alpha \Gamma(\mu)\overline{\gamma}^\mu} \exp\left(-\mu(\kappa+1)\frac{\gamma}{\overline{\gamma}}\right) \\ & \times {}_1F_1\left(\alpha;\mu;\frac{\mu^2\kappa(\kappa+1)\gamma}{(\mu\kappa+\theta)\overline{\gamma}}\right), \end{aligned} \tag{15}$$

in which $\overline{\gamma}$ denotes the corresponding average SNR.

3.5 | Moment Generating Function

The moment generating function (MGF) of the $\kappa-\mu$/GR distribution can be obtained from (15) by using the Laplace transformation $M_\gamma(s) = \mathscr{L}\left[f_\gamma(\gamma); -s\right]$, by using the Laplace transform frequency shifting and linearity properties, the transformation yields

$$\begin{aligned} M_\gamma(s) = {} & \frac{\mu^\mu \theta^\alpha (\kappa+1)^\mu}{(\mu\kappa+\theta)^\alpha \Gamma(\mu)\overline{\gamma}^\mu} \\ & \times \mathscr{L}\left[\gamma^{\mu-1}\, {}_1F_1\left(\alpha,\mu;\frac{\mu^2\kappa(\kappa+1)\gamma}{(\mu\kappa+\theta)\overline{\gamma}}\right); \frac{\mu(\kappa+1)}{\overline{\gamma}} - s\right]. \end{aligned} \tag{16}$$

The Laplace transform in (16) is obtained using the transformation pair [38, eq. (4.23.1)], and after some straightforward algebraic manipulations, the closed-form MGF expression is given as

$$\begin{aligned} M_\gamma(s) = {} & \frac{\mu^\mu \theta^\alpha (\kappa+1)^\mu}{(\mu\kappa+\theta)^\alpha \Gamma(\mu)\overline{\gamma}^\mu} \cdot \frac{\Gamma(\mu)}{(-s)^\mu} \\ & \times \left(1 - \frac{\mu(\kappa+1)}{s\overline{\gamma}}\right)^{-(\mu-\alpha)} \left(1 - \frac{\mu\theta(\kappa+1)}{(\mu\kappa+\theta)s\overline{\gamma}}\right)^{-\alpha}. \end{aligned} \tag{17}$$

3.6 | Cumulative Distribution Function

The cumulative distribution function (CDF) of the $\kappa-\mu$/GR distribution can readily be obtained using the MGF expression in (17) by using the inverse Laplace transform $F_\gamma(\gamma) = \mathscr{L}^{-1}\left[\frac{M_\gamma(-s)}{s}; \gamma\right]$, which yields

$$F_\gamma(\gamma) = \mathscr{L}^{-1}\left[\frac{\mu^\mu\theta^\alpha(\kappa+1)^\mu\Gamma(\mu+1)}{(\mu\kappa+\theta)^\alpha\Gamma(\mu)\bar{\gamma}^\mu}\cdot\frac{\Gamma(\mu)}{(s)^{\mu+1}}\left(1+\frac{\mu(\kappa+1)}{s\bar{\gamma}}\right)^{-(\mu-\alpha)}\left(1+\frac{\mu\theta(\kappa+1)}{(\mu\kappa+\theta)s\bar{\gamma}}\right)^{-\alpha};\gamma\right]. \tag{18}$$

The Laplace transform in (18) is obtained using the transformation pair [38, eq. (4.24.3)], and after some straightforward algebraic manipulations the closed-form CDF expression is given as

$$F_\gamma(\gamma) = \frac{\mu^{\mu-1}\theta^\alpha(\kappa+1)^\mu}{(\mu\kappa+\theta)^\alpha\Gamma(\mu)}\left(\frac{\gamma}{\bar{\gamma}}\right)^\mu \times\Phi_2\left(\mu-\alpha,\alpha;\mu+1;-\frac{\mu(\kappa+1)\gamma}{\bar{\gamma}},-\frac{\mu\theta(\kappa+1)\gamma}{(\mu\kappa+\theta)\bar{\gamma}}\right), \tag{19}$$

in which $\Phi_2(\cdot,\cdot,\cdot;\cdot,\cdot)$ is the dual variable hypergeometric Humbert Φ_2 function.

3.7 | Moments and Amount of Fading

The moments of the $\kappa-\mu$/GR distribution can be obtained using the SNR PDF expression in (15) by evaluating the integral $E[\gamma^n]=\int_0^\infty \gamma^n f_\gamma(\gamma)d\gamma$, which yields

$$E\left[\gamma^n\right] = \frac{\theta^\alpha\mu^\mu(\kappa+1)^\mu}{(\mu\kappa+\theta)^\alpha\Gamma(\mu)\bar{\gamma}^\mu}\int_0^\infty \gamma^{\mu+n-1} \times\exp\left(-\mu(\kappa+1)\frac{\gamma}{\bar{\gamma}}\right){}_1F_1\left(\alpha;\mu;\frac{\mu^2\kappa(\kappa+1)\gamma}{(\mu\kappa+\theta)\bar{\gamma}}\right). \tag{20}$$

The integral in (20) can be expressed in closed-form with the aid of [39, eq. (7.621.4)]. After some long but straightforward algebraic manipulations, the closed-form expression of the n^{th} order moments is given as

$$E\left[\gamma^n\right] = \frac{\bar{\gamma}^n\theta^\alpha\Gamma(n+\mu)}{\mu^n(\mu\kappa+\theta)^\alpha\Gamma(\mu)(\kappa+1)^n} \times{}_2F_1\left(\alpha,n+\mu;\mu;\frac{\mu\kappa}{\mu\kappa+\theta}\right), \tag{21}$$

in which ${}_2F_1(\cdot,\cdot;\cdot;\cdot)$ is the Gaussian hypergeometric function. It is recalled that the AF is a critical performance metric which indicates the severity of fading in a communication system. The AF is defined as

$$\mathrm{AF} = \frac{E\left[\gamma^2\right]}{(E[\gamma])^2} - 1. \tag{22}$$

Letting $n=1$ and $n=2$ in (21), the corresponding first-order $\mathbb{E}[\gamma]$ and second-order $\mathbb{E}\left[\gamma^2\right]$ moments are obtained, respectively, and with the aid of (22), the AF is given by

$$AF = \frac{(\mu+1)(\mu\kappa+\theta)^\alpha{}_2F_1\left(\alpha,\mu+2;\mu;\frac{\mu\kappa}{\mu\kappa+\theta}\right)}{\theta^\alpha\Gamma(\mu+1)\left[{}_2F_1\left(\alpha,\mu+1;\mu;\frac{\mu\kappa}{\mu\kappa+\theta}\right)\right]^2} - 1. \tag{23}$$

4 | Special Cases and Approximations

The closed-form PDF expression of the $\kappa-\mu$/GR composite fading model given by (14) describes the received faded signal envelope, R, for which the multipath propagation behavior is modelled by the $\kappa-\mu$ distribution. In (14), the resultant dominant signal components are randomly varied according to the GR distribution, as such, the composite fading model is indeed versatile since it inherits all of the generality of the $\kappa-\mu$ fading model, and therefore will find application in other areas of communications.

In (14), the amount of shadowing is controlled by the α parameter; this means as α approaches zero, $\alpha\to 0$, the dominant components are completely shadowed in (14). In contrast, as α approaches infinity, $\alpha\to\infty$, there is no shadowing present, and in this case, the PDF in (14) coincides with the $\kappa-\mu$ PDF as shown in Figure 2. In a similar manner, by setting $\mu=1$ and again letting $\alpha\to\infty$, the PDF in (14) coincides with the Rice PDF where the κ parameter becomes equivalent to the Rice K factor. The Rayleigh PDF can be readily obtained from the deduced Rice PDF by setting $\kappa=K=0$. Likewise, the Nakagami-m PDF can be deduced from (14) by letting $\alpha\to\infty$ and $\kappa\to 0$, where the μ parameter becomes equivalent to the m parameter of the Nakagami-m PDF. Table 1 provides

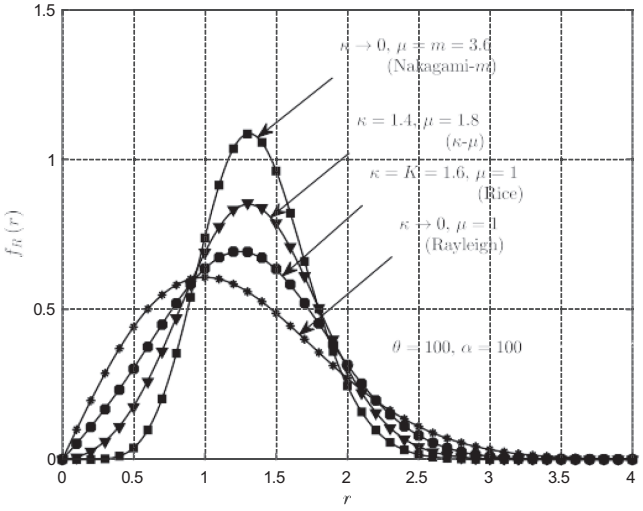

FIGURE 2 | PDF of the $\kappa-\mu$/gamma-Rayleigh composite fading model (continuous line) shown for various special cases of Nakagami-m (square markers), $\kappa-\mu$ (circle markers), Rayleigh (asterisk markers), and Rice (triangle markers) PDFs.

TABLE 1 | Summary of special cases of the $\kappa-\mu$/gamma-Rayleigh composite fading model.

	$\kappa-\mu$/gamma-Rayleigh $(\kappa,\mu,\theta,\alpha)$
One-sided Gaussian (θ)	$\kappa\to 0,\mu=0.5,\alpha\to\infty,\theta=\theta$
Rayleigh (θ)	$\kappa\to 0,\mu=1,\alpha\to\infty,\theta=\theta$
Rice (K,θ)	$\kappa=K,\mu=1,\alpha\to\infty,\theta=\theta$
Nakagami-m (m,θ)	$\kappa\to 0,\mu=m,\alpha\to\infty,\theta=\theta$
$\kappa-\mu$ (κ,μ,θ)	$\kappa=\kappa,\mu=\mu,\alpha\to\infty,\theta=\theta$

a summary of the special cases of the classical fading models that coincide with the $\kappa-\mu$/GR composite fading model for various parameters.

It is worth highlighting that, from the proposed $\kappa-\mu$/GR composite fading model, other composite fading models can be deduced where shadowing fading behavior is modelled according to the GR distribution in (6). As shown in Figure 3, examples of such composite fading models include the Rice/GR composite PDF ($\mu=1$), the Rayleigh/GR composite PDF ($\kappa=0$ and $\mu=1$) and the Nakagami/GR composite PDF ($\kappa=0$). The various special cases shown in Figure 3 can be obtained by varying the κ, μ, θ and α parameters of the proposed $\kappa-\mu$/GR PDF.

Classical composite fading models are typically based on the lognormal and inverse Gaussian shadowing models, which have found widespread applications in various studies in the literature. It is therefore beneficial to establish a comparison between the proposed LOS shadowed $\kappa-\mu$/GR model and classical LOS shadowed such as Rice/lognormal [3] and Rice/inverse Gaussian [40]. For these comparisons, the θ and α parameters of the proposed composite fading model were estimated from the classical lognormal and inverse Gaussian composite fading models by matching the moments of the respective shadowing distribution. The approach taken is to use the definitions of the method of moments (MoM) estimators of the α and θ parameters of the GR model, and substitute the closed-form expressions of the respective n^{th} order moments of the lognormal and inverse Gaussian models. In the literature, the typical approach is to match the n^{th} order moments of a newly proposed composite fading model with the n^{th} order moments of the existing classical lognormal or inverse Gaussian shadowed composite fading models. However, this approach can be tedious and can sometimes lead to intractable solutions if the proposed models are not available in closed-form. Most classical multipath fading models can be directly obtained from the $\kappa-\mu$ PDF by appropriately setting the κ and μ parameters, this is usually not the case for shadowing models. Therefore, this approach has the advantage being directly applied to different shadowing models provided that there exists MoM estimators for their parameters, and it has the advantage of leading to closed-form solutions.

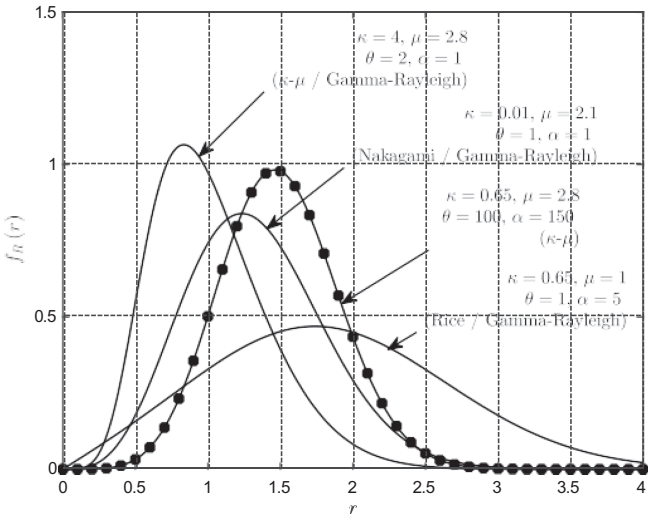

FIGURE 3 | PDF of the $\kappa-\mu$/gamma-Rayleigh composite fading model (continuous lines) for various values of κ, μ, α, and θ parameters. The circle markers represent the special case when the $\kappa-\mu$/gamma-Rayleigh PDF coincides to the $\kappa-\mu$ PDF.

The n^{th} order moments of the GR distributions are given by (24). Following the standard procedure of ratio of moments [41, 42] and letting $n=2$ and $n=4$ in (24), the second-order and fourth-order moments are obtained for GR accordingly.

$$u_n=\mathbb{E}\left[R^n\right]=\frac{\Gamma(\alpha+n/2)}{\Gamma(\alpha)\theta^{n/2}}. \tag{24}$$

Taking the ratio $\frac{u_4}{u_2}$ and solving for α and θ, the MoM estimators for the GR model are given as

$$\alpha=\frac{{u_2}^2}{u_4-{u_2}^2}, \tag{25}$$

and

$$\theta=\frac{u_2}{u_4-{u_2}^2}. \tag{26}$$

The n^{th} moments of the lognormal distribution are given by (27), substituting the appropriate second-order ($n=2$) and fourth-order ($n=4$) moment expressions for u_4 and u_2 into (25) and (26), the relationships between the α and θ parameters of the GR model, and the λ and σ parameters of the lognormal model are given by (28) and (29), respectively.

$$u_n=e^{n\lambda+\frac{1}{2}n^2\sigma^2}. \tag{27}$$

$$\alpha=\frac{1}{\exp\left(4\sigma^2\right)-1}. \tag{28}$$

$$\theta=\frac{\exp\left(-2\lambda-2\sigma^2\right)}{\exp\left(4\sigma^2\right)-1}. \tag{29}$$

The n^{th} moments of the inverse Gaussian distribution are given by (30), where $K_v(\cdot)$ denotes the modified Bessel function of the second kind of order v. Substituting the appropriate second-order ($n=2$) and fourth-order ($n=4$) moment expressions for u_4 and u_2 into (25) and (26), the relationships between the α and θ parameters of the GR model, and the η and ρ parameters of the inverse Gaussian model are given by (31) and (32), respectively.

$$u_n=e^{\frac{\rho}{\eta}}\sqrt{\frac{2\rho}{\pi}}\eta^{n-1/2}K_{1/2-n}\left(\frac{\rho}{\eta}\right). \tag{30}$$

$$\alpha=\frac{\rho(\eta+\rho)^2}{\eta\left(15\eta^2+14\eta\rho+4\rho^2\right)}. \tag{31}$$

$$\theta=\frac{\rho^2(\eta+\rho)}{\eta^3\left(15\eta^2+14\eta\rho+4\rho^2\right)}. \tag{32}$$

Using the expressions in (28) and (29), the $\kappa-\mu$/GR PDF can be used as an excellent approximation of Rice/lognormal PDF as shown in Figure 4. Similarly, using the expressions in (31) and (32), the $\kappa-\mu$/GR PDF can be used as an excellent approximation of the Rice/ inverse Gaussian model as shown in Figure 5. The derived parameter relationships are particularly useful for two reasons.

First, in the case whereby the new shadowing models are applied to measurements previously collected but the measurement data are not available for parameter estimation, the relationships can be used to obtain the parameters of the new shadowing models using published results. Second, the derived parameter relationships circumvent the need for the time-consuming nonlinear curve fitting procedures by allowing parameters of the new shadowing models to be quickly obtained using published results.

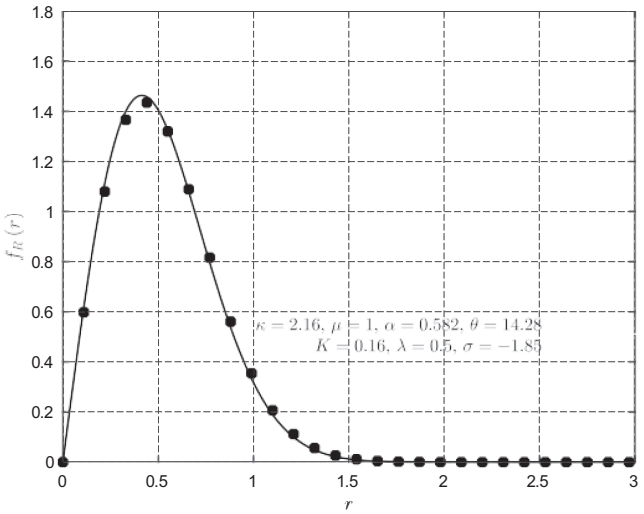

FIGURE 4 | PDF of the $\kappa-\mu$/gamma-Rayleigh composite fading model (continuous line) and approximation of the Rice/lognormal (circle markers) composite fading model.

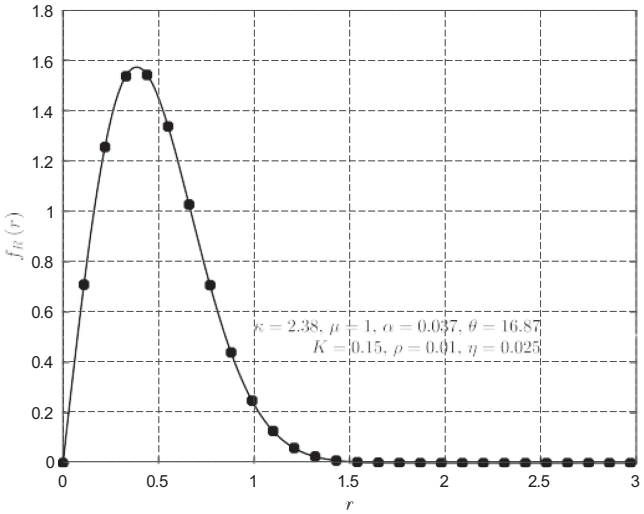

FIGURE 5 | PDF of the $\kappa-\mu$/gamma-Rayleigh composite fading model (continuous line) and approximation of the Rice/inverse Gaussian (circle markers) composite fading model.

5 | Performance Analysis

In this section, key performance metrics such as outage probability (OP), average symbol error probability (ASEP) and average channel capacity for communication systems operating over the $\kappa-\mu$/GR fading channel are derived. The closed-form expressions utilized to derive these measures are well established for fading channels with additive white Gaussian noise (AWGN) interference, which are typically found in wireless systems. In PLC systems, the noise interference in the communication channel is generally viewed as a combination of background noise and impulsive noise. Background noise, being wideband with a low power spectral density (PSD), is appropriately modelled as AWGN, whereas impulsive noise, is narrowband and occurs in bursts, and exhibits high PSD. Impulsive noise is usually observed in the tens of megahertz range [43] in PLC systems operating in indoor low-voltage (LV) power networks. However, since the measurements in this study are conducted at carrier frequencies in the hundreds of megahertz, the effects of impulsive noise can be safely avoided, and the noise interference in the hybrid PLCWLC channel can be effectively considered as AWGN.

5.1 | Outage Probability

The OP is a key performance metric for evaluating communication systems. It is defined as the probability that the instantaneous SNR, γ, of the received signal falls below a predefined threshold, γ_{th}, that is $P_{out}(\gamma \le \gamma_{th})$. Mathematically P_{out} is given as

$$P_{out} = \int_0^{\gamma_{th}} f_\gamma(\gamma)d\gamma, \tag{33}$$

which is equivalent to the CDF of the $\kappa-\mu$/GR model evaluated at γ_{th}, which is given as

$$F_\gamma(\gamma_{th}) = \frac{\mu^{\mu-1}\theta^\alpha(\kappa+1)^\mu}{(\mu\kappa+\theta)^\alpha\Gamma(\mu)}\left(\frac{\gamma}{\gamma_{th}}\right)^\mu \Phi_2\left(\mu-\alpha,\alpha;\mu+1;-\frac{\mu(\kappa+1)\gamma}{\gamma_{th}},-\frac{\mu\theta(\kappa+1)\gamma}{(\mu\kappa+\theta)\gamma_{th}}\right). \tag{34}$$

in which $\Phi_2(\cdot,\cdot,\cdot;\cdot,\cdot)$ is the dual variable hypergeometric Humbert Φ_2 function.

5.2 | Average Symbol Error Probability

The ASEP for various coherent modulation schemes over the $\kappa-\mu$/GR fading channel can be obtained as

$$P_e(\overline{\gamma}) = A_c\int_0^\infty \mathrm{erfc}\left(\sqrt{B_c\gamma}\right)f_\gamma(\gamma)d\gamma, \tag{35}$$

where $\mathrm{erfc}(\cdot)$ is the complementary error function and $f_\gamma(\gamma)$ is the SNR PDF given by the integral form in (36). A_c and B_c are constants and depend on the modulation schemes. $A_c = 0.5$ and $B_c = 1$ corresponds to BPSK modulation, and $A_c = 1$ and $B_c = 0.5$ corresponds to QPSK modulation.

$$f_\gamma(\gamma)= \frac{2\mu\theta^{\alpha}(\kappa+1)^{\frac{\mu+1}{2}}\gamma^{\frac{\mu-1}{2}}}{\kappa^{\frac{\mu-1}{2}}\Gamma(\alpha)\bar{\gamma}^{\frac{\mu+1}{2}}\exp\left(\frac{\mu(\kappa+1)\gamma}{\bar{\gamma}}\right)} \int_0^{\infty} z^{2\alpha-\mu}\exp\left(-(\mu\kappa+\theta)z^2\right) I_{\mu-1}\left(2\mu\sqrt{\frac{\kappa(\kappa+1)\gamma}{\bar{\gamma}}}z\right)dz. \tag{36}$$

Substituting (36) into (35) yields

$$P_e(\bar{\gamma})= \frac{A_c 2\mu\theta^{\alpha}(\kappa+1)^{\frac{\mu+1}{2}}}{\kappa^{\frac{\mu-1}{2}}\Gamma(\alpha)\bar{\gamma}^{\frac{\mu+1}{2}}} \int_0^{\infty} z^{2\alpha-\mu}\exp\left(-(\mu\kappa+\theta)z^2\right) \times \int_0^{\infty} \gamma^{\frac{\mu-1}{2}}\operatorname{erfc}\left(\sqrt{B_c\gamma}\right)\exp\left(-\frac{\mu(\kappa+1)\gamma}{\bar{\gamma}}\right) I_{\mu-1}\left(2\mu\sqrt{\frac{\kappa(\kappa+1)\gamma}{\bar{\gamma}}}z\right)d\gamma dz. \tag{37}$$

Using the series representation of the function $I_v(\cdot)$ given by [39, eq. (8.445)], and using the Laplace transform pair [44, eq. (3.7.2.5)] along with some basic algebraic manipulation yields

$$P_e(\bar{\gamma})= \frac{A_c 2\mu^{\mu}\theta^{\alpha}(\kappa+1)^{\mu}}{\sqrt{\pi}\Gamma(\alpha)\left(B_c\bar{\gamma}\right)^{\mu}} \sum_{i=0}^{\infty} \frac{\mu^{2i}\kappa^i(\kappa+1)^i\Gamma\left(\mu+i+\frac{1}{2}\right)}{\left(B_c\bar{\gamma}\right)^i\Gamma(\mu+i+1)i!} \times {}_2F_1\left(\mu+i,\mu+i+\frac{1}{2};\mu+i+1;-\frac{\mu(\kappa+1)}{B_c\bar{\gamma}}\right) \int_0^{\infty} z^{2\alpha-1-2i}\exp\left(-(\mu\kappa+\theta)z^2\right)dz. \tag{38}$$

Using [39, eq. (3.326.2)], the ASEP is given as

$$P_e(\bar{\gamma})= \frac{A_c\mu^{\mu}\theta^{\alpha}(\kappa+1)^{\mu}}{\sqrt{\pi}\Gamma(\alpha)\left(B_c\bar{\gamma}\right)^{\mu}(\mu\kappa+\theta)^{\alpha}} \sum_{i=0}^{\infty} \frac{\mu^{2i}\kappa^i(\kappa+1)^i\Gamma\left(\mu+i+\frac{1}{2}\right)\Gamma(\alpha+i)}{\left(B_c\bar{\gamma}\right)^i\Gamma(\mu+i+1)(\mu\kappa+\theta)^i i!} {}_2F_1\left(\mu+i,\mu+i+\frac{1}{2};\mu+i+1;-\frac{\mu(\kappa+1)}{B_c\bar{\gamma}}\right), \tag{39}$$

in which ${}_2F_1(\cdot,\cdot;\cdot;\cdot)$ denotes the Gaussian hypergeometric function.

5.3 | Average Channel Capacity

For an AWGN fading channel, the instantaneous capacity is given by $C_{AWGN} = \left(1/\ln(2)\right)\ln(1+\gamma)$, where γ represents the received SNR. To determine the average channel capacity C of the $\kappa-\mu$/GR fading channel, the C_{AWGN} expression is averaged over the instantaneous SNR PDF as

$$C = \frac{1}{\ln(2)}\int_0^{\infty} f_\gamma(\gamma)\ln(1+\gamma)d\gamma. \tag{40}$$

Substituting the integral form of the instantaneous SNR PDF given by (36) into (40) yields

$$C= \frac{2\mu\theta^{\alpha}(\kappa+1)^{\frac{\mu+1}{2}}}{\ln(2)\kappa^{\frac{\mu-1}{2}}\Gamma(\alpha)\bar{\gamma}^{\frac{\mu+1}{2}}} \int_0^{\infty} z^{2\alpha-\mu}\exp\left(-(\mu\kappa+\theta)z^2\right) \times \int_0^{\infty} \gamma^{\frac{\mu-1}{2}}\ln(1+\gamma)\exp\left(-\frac{\mu(\kappa+1)\gamma}{\bar{\gamma}}\right) I_{\mu-1}\left(2\mu\sqrt{\frac{\kappa(\kappa+1)\gamma}{\bar{\gamma}}}z\right)d\gamma dz. \tag{41}$$

Using the series representation of the $I_v(\cdot)$ function given by [39, eq. (8.445)], and using the Laplace transform pair [44, eq. (2.5.2.11)] along with some basic algebraic manipulation yields

$$C= \frac{2\mu\theta^{\alpha}}{\ln(2)\Gamma(\alpha)} \sum_{i=0}^{\infty} \frac{\mu^i\kappa^i}{\Gamma(\mu+i)i!} G_{3,2}^{1,3}\left(\frac{\bar{\gamma}}{\mu(\kappa+1)}\middle| \begin{matrix}1-\mu-i,1,1\\1,0\end{matrix}\right) \int_0^{\infty} z^{2\alpha-1-2i}\exp\left(-(\mu\kappa+\theta)z^2\right)dz, \tag{42}$$

in which $G_{p,q}^{m,n}(z|\cdots)$ denotes the Meijer G function. Using [39, eq. (3.326.2)] to solve the integral and using the Meijer G function property [45, eq. (8.2.2.14)], the average channel capacity is given as

$$C= \frac{\theta^{\alpha}}{\ln(2)\Gamma(\alpha)(\mu\kappa+\theta)^{\alpha}} \sum_{i=0}^{\infty} \frac{\mu^i\kappa^i\Gamma(\alpha+i)}{\Gamma(\mu+i)(\mu\kappa+\theta)^i i!} G_{2,3}^{3,1}\left(\frac{\mu(\kappa+1)}{\bar{\gamma}}\middle| \begin{matrix}0,1\\\mu+i,0,0\end{matrix}\right). \tag{43}$$

6 | Numerical Results

In this section, the closed-form analytical results obtained in the previous section for the proposed composite fading model are used to study the impact of different channel parameters and provide representative numerical examples of the performance measures of interest. The validity of the derivations of the OP, ASEP and average channel capacity metrics given by (34), (39), and (43), respectively, is demonstrated by plotting the numerical results along with the Monte Carlo simulations generated from 10_7 realizations. Without loss of generality, in all the results presented here $\alpha = \theta$, which means that the mean power of the fading channel is unity.

Figure 6 shows the OP performance versus the average SNR $\bar{\gamma}$ for various fading parameters $[\kappa,\mu,\theta,\alpha]$ at a threshold value of $\gamma_{th} = 5$ dB. It can observed that the analytical curves generated by (34) are in good agreement with the Monte Carlo simulations over the entire SNR regime. In generating the analytical curves, the numerical computation of the dual variable Hypergeometric Humbert Φ_2 function was done using [46, eq. (4.19)] which is a very appropriate ${}_1F_1$ series representation of the Φ_2 function. From Figure 6, it can be observed that the OP improves as the parameters κ, μ and α increases. This can attributed to the following reasons. The κ parameter represents the strength of

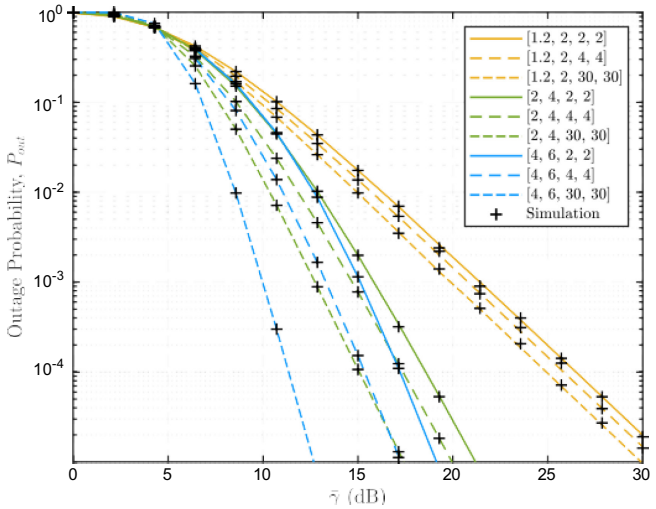

FIGURE 6 | Outage probability versus the average SNR $\bar{\gamma}$ for various fading parameters $[\kappa, \mu, \theta, \alpha]$ of the $\kappa - \mu$/GR channel at a threshold value of $\gamma_{th} = 5$ dB.

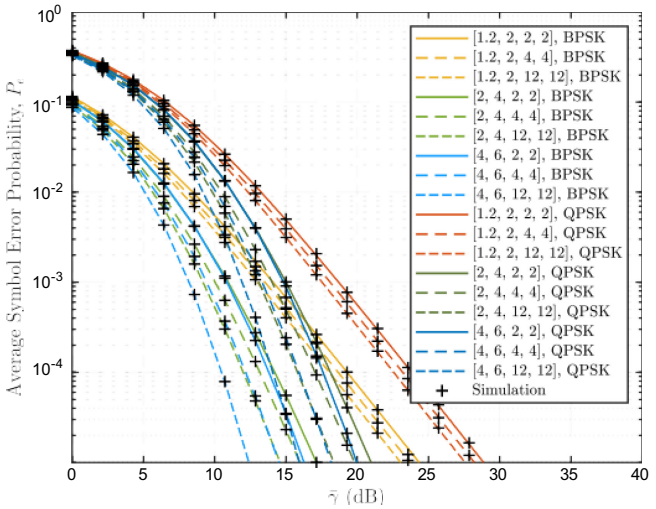

FIGURE 7 | ASER performance of BPSK and QPSK versus the average SNR $\bar{\gamma}$ for various fading parameters $[\kappa, \mu, \theta, \alpha]$ of the $\kappa - \mu$/GR channel.

the LOS component, as the LOS component increases, the received signal strength increases and is less likely to fall below the predefined threshold, thus OP improves. The μ parameter represents the number of clusters of multipath components, as μ increases there is increased signal diversity which means that the number of replicas of the same transmitted signal that reach the receiver improves, and as a result OP improves. The α parameter represents the severity of fading and holds an inverse relationship, as such $\alpha = 2$ represents heavy shadowing, $\alpha = 4$ represents moderate shadowing and $\alpha = 30$ represent light shadowing. Therefore, it is evident that low values of α represent more shadowing and a poor OP performance, on the other hand high values of α represent less shadowing and an improved OP performance.

Figure 7 shows the ASEP performance versus the average SNR $\bar{\gamma}$ for various fading parameters $[\kappa, \mu, \theta, \alpha]$. The ASEP is computed for BPSK modulation by setting $A_c = 0.5$ and $B_c = 1$ in (39), and for QPSK modulation by setting $A_c = 1$ and $B_c = 0.5$ in (39). From Figure 7, it can observed that the analytical curves generated by (39) are in good agreement with the Monte Carlo simulations over the entire SNR regime. QPSK modulation has a higher constellation than BPSK modulation, therefore it is expected that QPSK will exhibit higher error probabilities than BPSK. However, it can be observed that in the high SNR range QPSK can obtain better performance than BPSK for larger parameter values. In general, an improvement in the error rates can be observed for both BPSK and QPSK modulations as the parameters increase. These improvements can be attributed to the same reasons of increased LOS component, increased signal diversity due to multipath propagation and shadowing severity as explained previously.

Figure 8 shows the channel capacity versus the average SNR $\bar{\gamma}$ for various fading parameters $[\kappa, \mu, \theta, \alpha]$. It can observed that the analytical curves generated by (43) are in good agreement with the Monte Carlo simulations over the entire SNR regime. From Figure 8, it can be observed that for fixed κ and μ values, the channel capacity improves with an increase in α value, and

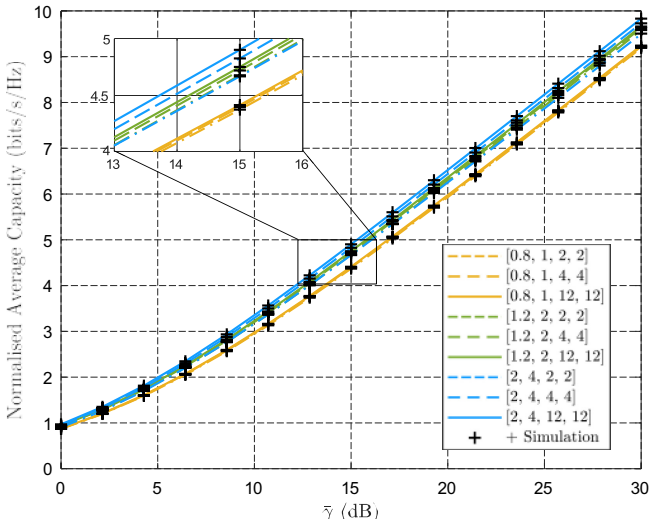

FIGURE 8 | Average channel capacity versus the average SNR $\bar{\gamma}$ for various fading parameters $[\kappa, \mu, \theta, \alpha]$ of the $\kappa - \mu$/GR channel.

there is a general improvement of the channel capacity with an increase of the parameters. Similarly, these improvements can be attributed to the same reasons of increased LOS component, increased signal diversity due to multipath propagation and shadowing severity as explained previously.

7 | Channel Setup and Measurements

Channel measurements for hybrid PLC-WLC communication channels were conducted for two different indoor propagation environments. The first environment considered was an office hallway, which was designated as a small-indoor environment. The second environment considered was a lecture hall foyer, which was denoted as a large-indoor environment. The small-indoor and large-indoor environments used to obtain the measurements are located on the 15^{th} and 1^{st} floor, respectively, of the Engineering 1 building at the University of Pretoria in Pretoria, South Africa. The

floor layouts of the small-indoor and large-indoor environments are shown in Figures 9 and 10, respectively. For both environments, hybrid PLC-WLC channel measurements were performed for three different channel scenarios categorized by the branching characteristics of the PLC portion of the hybrid PLC-WLC channel. The PLC channel in each scenario was constructed using the H05RR-F 3-Core (0.75 mm^2) cable-type which is typically found in indoor low-voltage (LV) power networks.

For the first measurement scenario, the PLC channel had multiple branches (MB) as shown in the lower part of Figure 9 and the upper part of Figure 10, this channel was unknown since some electrical outlets were left open and other outlets had small common household appliances connected to represent different loads. Moreover, the absolute distances between branches are unknown. For the second measurement scenario, the PLC channel was constructed with two branches (TB) with connections between points *A*, *C*, which was left open, *B* and *D* which was left open. For the third measurement scenario, the PLC channel was made up of a single cable forming a single branch (SB) between points *A* and *D* in the small-indoor environment and the large-indoor environment. The lower part of Figure 9 and the upper part of Figure 10 show a wall in the respective environment where the experimental PLC portion of the hybrid PLC-WLC channel was set-up, which is representative of indoor wiring practices. In both figures, shown in the PLC channels is a (■) which represents a branch, (○) denotes an open connection and (•) represents a load connected in the network. For all the scenarios considered, the PLC channel was set up to have a total length of 20 and 16 m between points *A* and *D* for the small-indoor and large-indoor environment, respectively, along the wall length in the respective environment. The following should be noted about the constructed PLC channels: (i) each terminal point only has a single node whether open or with load connected, (ii) there are no connections between termination points and (iii) the channel has a radial topology with no loops.

The transmitter (TX) for all measurement scenarios considered, consisted of a Nuand BladeRF Micro A4 which was configured to transmit a continuous wave (CW) signal with an output power of +6 dBm at 433 MHz. The CW signal was injected into the PLC channel at point *A* using a capacitive coupling circuit and the TX remained stationary for each measurement scenario in both environments. The receiver (RX) also consisted of a Nuand BladeRF Micro A4 with a 433 MHz ISM band antenna connected to the BladeRF receiver port. GNU Radio platform was used to control the TX and RX BladeRF SDRs. The RX was configured to have a sampling rate of 2.6 Mbps and a bandwidth of 800 kHz centered at 433 MHz. The measurements samples were collected and stored on external memory. In GNU Radio, the stored samples were decimated to a lower frequency of 26 KHz and low-pass filtered to 10 KHz, this is comprehensible since the focus of this study is the time-selective behavior

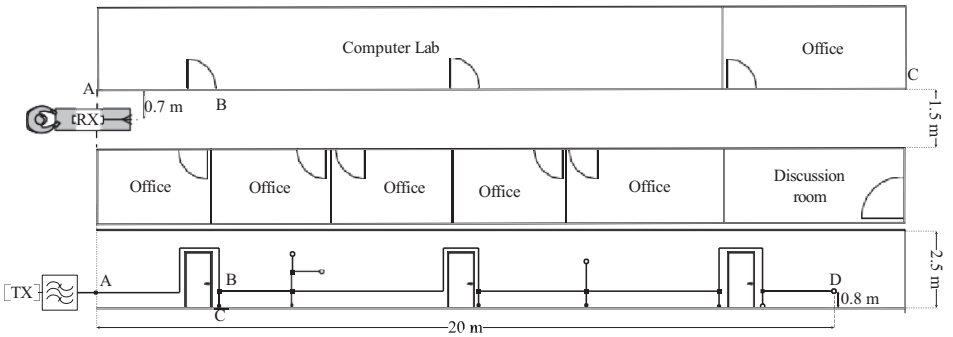

FIGURE 9 | Experimental PLC-WLC channel setup in office hallway environment (small-indoor).

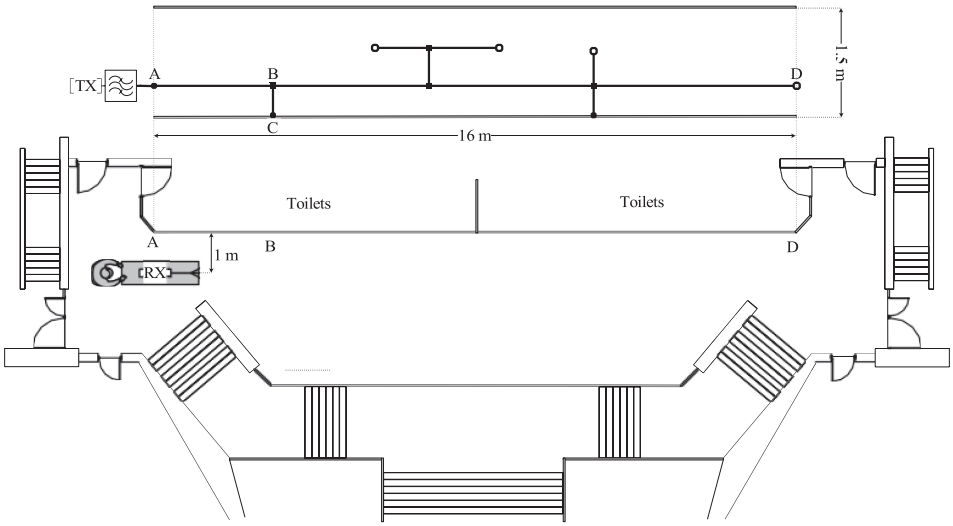

FIGURE 10 | Experimental PLC-WLC channel setup in lecture hall foyer environment (large-indoor).

of the hybrid PLC-WLC channel, and therefore narrowband measurements are required. The RX antenna was placed at the same height as the points A and D in all scenarios, and placed 0.7 m away from the PLC channel in the small-indoor environment and 1 m away from the PLC channel in the large-indoor environment. The TX was continuously injecting the CW signal, and the samples were collected while the RX was pushed on a trolley along the PLC channel path in a straight line at an approximate constant velocity v of 2.5 m s_{-1}. To this end, the collected time-series t measurements were converted to the distance series x measurements using the relationship $x = vt$.

Another aspect to be considered is signal path-loss, which is related to the gradual loss of the mean level signal strength with the signal propagation path. In wireless channels, path-loss measurements are typically obtained with the receiver moving along an arbitrary path, or in a circular route around the transmitter or at arbitrary locations in the propagation environment. Another approach is to use linear regression methods to estimate path-loss from the long-term (shadow) fading signal component. The regression analysis depend on the path-loss function adopted, because various shadow fading models can be used, the estimated path-loss can vary considerably [47]. The unique propagation characteristics of the hybrid PLC-WLC channel environment does not allow for direction application of established wireless channel linear regression methods. Moreover, there is no established path-loss model for a hybrid PLC-WLC channel. Therefore, path-loss for the hybrid PLC-WLC channel was estimated empirically by conducting measurements at fixed positions along the propagation path along the length of the wall in the small-indoor and large-indoor environments. At each fixed position, multiple RX measurements were recorded for a fixed period. The fixed position measurements were averaged, and an average of the measurements was taken to obtain the path-loss value at the x position. The sparse path-loss values were then interpolated for the whole measurement path of 20 m of the small-indoor environment and 16 m of the large-indoor environment. Having the interpolated path-loss values, the initial step in processing the received composite faded signal envelope was to eliminate the path-loss effects imparted by the propagation environment on the received signal. Post-processing of the composite faded signal was done in MATLAB, and a non-linear least squares routine was programmed in MATLAB to fit the proposed composite fading model to the received composite faded signal for each measurement scenario in both environments.

8 | Results and Discussions

The results of the small-indoor environment measurements fitting to the proposed $\kappa-\mu$/GR composite fading model are shown in Figure 11a–c for the SB, TB and MB scenarios, respectively. Similarly, the results of the large-indoor environment measurements fitting to $\kappa-\mu$/fading GR model are shown in Figure 12a–c for the SB, TB and MB scenarios, respectively. In addition to the proposed $\kappa-\mu$/GR fading model, the LOS shadowed Rice/Nakagami-m [48] fading model, and the multiplicative shadowed $\kappa-\mu$/inverse gamma [17] and

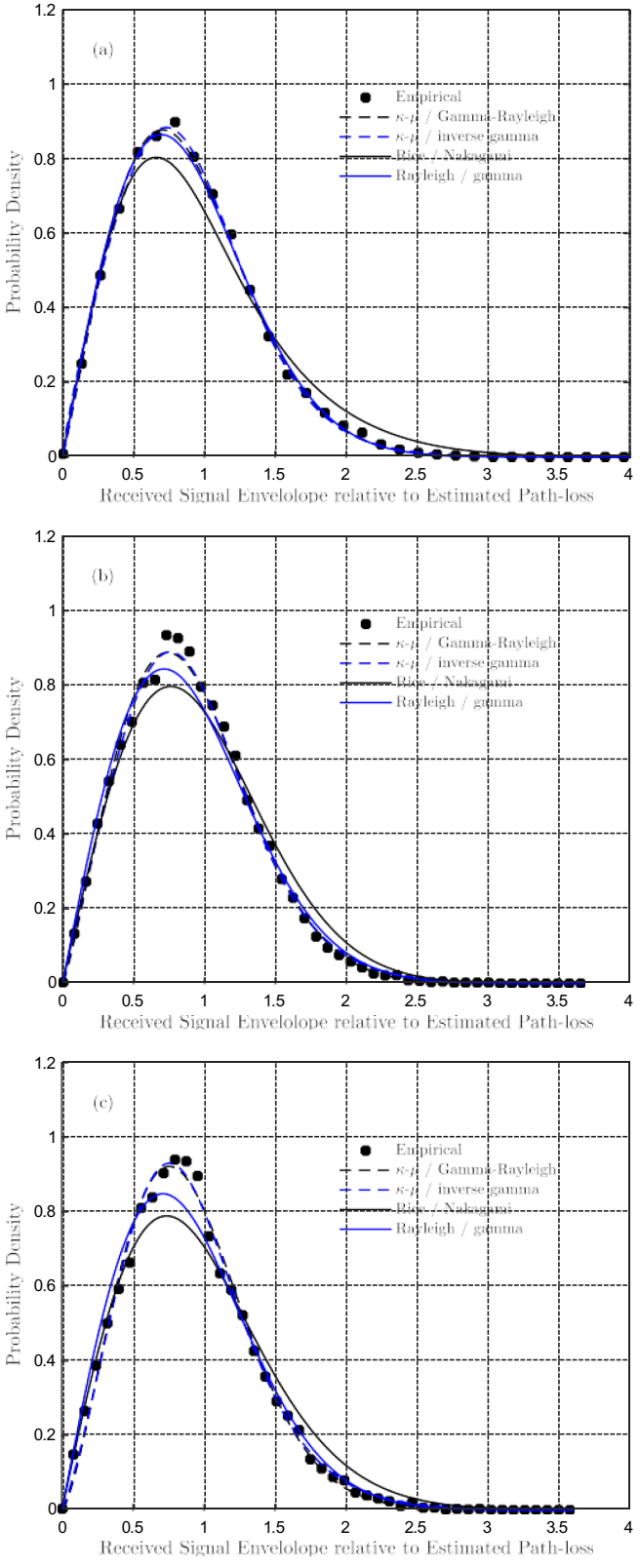

FIGURE 11 | Empirical PDFs (circle markers) of the received composite faded signal observed in the PLC-WLC channel in the office hallway environment for the (a) SB scenario, (b) TB scenario, and (c) MB scenario compared to the theoretical $\kappa-\mu$/gamma-Rayleigh, $\kappa-\mu$/inverse gamma, Rice/Nakagami and Rayleigh/gamma composite fading models.

Rayleigh/gamma (K-distribution) [4] fading models were included in the fitting process for comparative purposes as shown in Figures 11 and 12. Shown in both figures are the plots of the empirical PDFs, and the composite fading models are shown with their corresponding plot labels. The goodness-of-fit for each composite fading model was evaluated using the Kullback-Leibler (KL) divergence test. The KL test statistic is defined as

$$D_{KL} = \int_0^\infty P(x) \ln\left(\frac{P(x)}{\hat{P}(x)}\right) dx, \tag{44}$$

which is described as the relative entropy or distance between the empirical PDF $\hat{P}(x)$ and the theoretical PDF $P(x)$. Since the D_{KL} metric gives a measure of how much information is lost when $\hat{P}(x)$ is used to approximate $P(x)$, the lowest D_{KL} value indicates the most favorable distribution for modelling the received composite faded signal.

Table 2 shows the estimated parameters and results of the KL test for each propagation environment and for each PLC-WLC measurement scenario. For the small-indoor propagation environment, it can be observed from the plots of Figure 11 that the proposed $\kappa-\mu$/GR model exhibited excellent fit to the measurements, and the $\kappa-\mu$/inverse gamma also showed good fit to the measurements. The small-indoor environment can be considered to be a rich scattering environment that exhibits multipath propagation clustering behavior, which is indicated by the estimated $\mu > 1$ parameter for both composite fading models for almost all PLC-WLC scenarios. This also suggests that the random fluctuations of the received signal are largely due to the rich scattering behavior of the environment. It can be observed from the D_{KL} values that the $\kappa-\mu$/inverse gamma fading model obtained the best performance for the TB and MB propagation scenarios, while the $\kappa-\mu$/GR fading model obtained the best performance for the SB scenario. This suggests that significant measurable shadowing of both the dominant signal component and scattered components was found to exists in the TB and MB scenarios. These results suggest that the total power of the scattered components is likely to have been significant, and therefore impacted the power of dominant signal components. The estimated α parameter of the $\kappa-\mu$/GR fading model indicate that the shadowing severity increases in the order of SB, MB, and TB scenarios, which is corroborated by the decrease of the estimated κ parameter in the same order. While the estimated α parameter of the $\kappa-\mu$/ inverse gamma model indicates that the shadowing severity increases in the order of SB, TB and MB scenarios, which is corroborated by the decrease of the estimated κ in the same order. Moreover, the increase in shadowing severity in the order of SB, TB and MB is further corroborated by the decrease of Rice K factor and the Rayleigh/gamma fading model β parameter in the same order. The total power of the scattered multipath components increases in order of SB, TB, and MB scenarios, as reflected by the increase of the Rayleigh/gamma model σ parameter in the same order. According to the D_{KL} values, the Rice/Nakagami model obtained the worst performance in all scenarios, this model is a LOS shadowed model

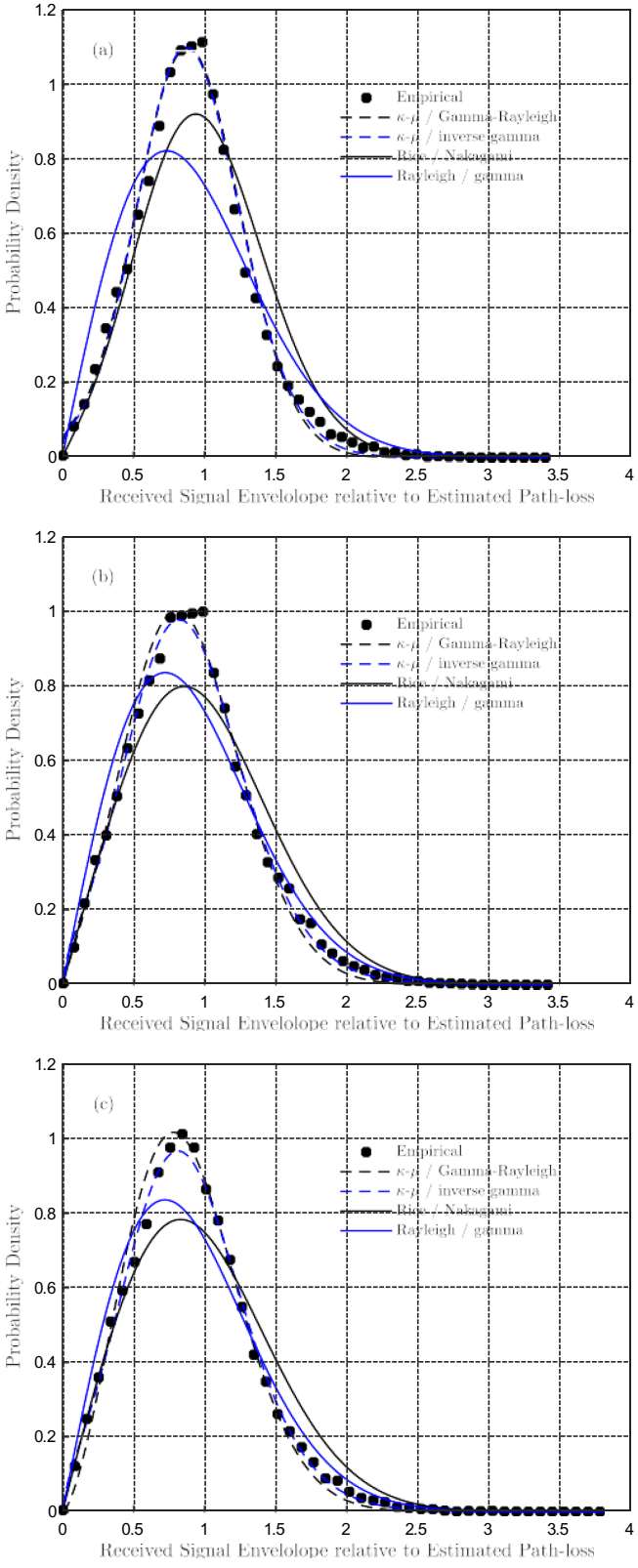

FIGURE 12 | Empirical PDFs (circle markers) of the received composite faded signal observed in the PLC-WLC channel in the lecture hall foyer environment for the (a) SB scenario, (b) TB scenario, and (c) MB scenario compared to the theoretical $\kappa-\mu$/gamma-Rayleigh, $\kappa-\mu$/inverse gamma, Rice/Nakagami and Rayleigh/gamma composite fading models.

TABLE 2 | Parameter estimates for the $\kappa-\mu$/gamma-Rayleigh, $\kappa-\mu$/inverse gamma, Rice/Nakagami and Rayleigh/gamma composite fading models for office hallway and lecture hall foyer environment PLC-WLC propagation scenarios.

LOS shadowing composite fading									
		$\kappa-\mu$/gamma-Rayleigh					**Rice/Nakagami**		
		κ	μ	θ	α	D_{KL}	K	m	D_{KL}
Office hallway	MB	0.2399	1.2026	0.0034	0.0048	0.0066	0.5533	0.5000	0.0239
	TB	0.1510	1.1007	1.7326	0.0016	0.0023	1.0358	1.0035	0.0142
	SB	0.3218	1.0408	0.1140	0.0299	0.0015	1.1000	0.3728	0.0225
Lecture hall foyer	MB	4.2911	1.2659	2.2521	1.5542	0.085	1.8000	1.2808	0.0300
	TB	8.3307	0.9658	2.3710	1.7187	0.0031	3.0000	1.3137	0.0294
	SB	9.1714	0.6598	5.4488	4.1725	0.0131	5.0000	2.1140	0.0322
Multiplicative shadowing composite fading									
		$\kappa-\mu$/ inverse gamma					**Rayleigh/gamma**		
		κ	μ	β	α	D_{KL}	σ	β	D_{KL}
Office hallway	MB	0.9990	1.1060	0.8778	6.0000	0.0052	0.0528	90.9166	0.0077
	TB	1.0118	0.9951	0.9099	7.6500	0.0034	0.0519	95.1645	0.0048
	SB	1.1000	0.9070	0.8680	8.0000	0.0018	0.0495	99.6324	0.0020
Lecture hall foyer	MB	2.11	0.8460	0.8949	10.6073	0.0021	0.0518	97.3171	0.0159
	TB	2.4679	0.8040	0.8904	10.7456	0.067	0.0513	99.3140	0.0182
	SB	5.0240	0.6108	0.9120	22.3919	0.0264	0.0510	103.9249	0.0551

and these results can also be attributed to the rich scattering nature of the propagation environment.

For the large-indoor environment, it can be observed from the plots in Figure 12 that both the $\kappa-\mu$/GR and the $\kappa-\mu$/inverse gamma models exhibited excellent fit to the measurements. From Table 2, it can be observed from the D_{KL} values that the $\kappa-\mu/$ inverse gamma model obtained the best performance for the MB scenario, while the $\kappa-\mu$/GR model obtained the best performance for the TB and SB scenarios. This suggests that measurable shadowing of both the dominant signal component and scattered components was found to exists in MB scenario, while in the TB and SB scenarios the total power of the scattered signal components were found to be relatively so weak compared to that of the dominant signal components. Even though there is measurable shadowing in MB scenario, the large-indoor environment is not necessarily a rich scattering environment as indicated by the estimated $\mu < 1$ of the favorable $\kappa-\mu$/inverse gamma model for this scenario. This also suggests that more dominant signal components were present and actively contributed to the received signal, thereby increasingly stabilizing the received signal and reducing the random fluctuations caused by shadowing effects in the received signal. The estimated $\kappa > 1$ parameter in both models further corroborates that the total power of the scattered components is likely to have been less significant and had less impact on the power of LOS components. The estimated α parameters of the $\kappa-\mu$/GR model and the $\kappa-\mu$/inverse gamma model indicate that the shadowing severity increases in the order of SB, TB and MB scenarios, which is corroborated by the decrease of the estimated κ parameter in the same order of both models. Furthermore, the increase in shadowing severity in the order of SB, TB and MB is further corroborated by the decrease of Rice K factor and the Rayleigh/gamma fading model β parameter in the same order. The total power of the scattered multipath components increases in the order of SB, TB and MB scenarios, as reflected by the increase of the estimated Rayleigh/gamma model σ parameter in the same order. According to the D_{KL} values the Rice/Nakagami model obtained the worst performance in TB and MB scenarios, and outperformed the Rayleigh/gamma model in the SB scenario. These results can also be attributed to the fact that in the large-indoor environment SB scenario, more dominant signal components were present and there were less mean power random fluctuations in the received signal.

Based on the results of the fitting process, it is evident that a line-of-sight (LOS) shadowing composite fading model may be appropriate in certain scenarios, while a multiplicative shadowing composite fading model may be better suited for others. The $\kappa-\mu$ fading model, which assumes a clustered behavior of dominant and scattered components, suggests that in the $\kappa-\mu$/inverse gamma model, both the dominant and scattered signal components can be jointly shadowed. While this assumption holds in some cases, it can be argued that in other situations, the total power contribution from the scattered components, which are assumed to be shadowed, may be too weak to significantly influence the received signal. In such cases, the random fluctuations in the received signal are primarily determined by the shadowed dominant signal components. This distinction should be carefully considered for accurately modelling fading in

different propagation environments. Thus, the reasons for using the proposed LOS shadowed $\kappa - \mu$/fading model and comparing it with the existing multiplicative shadowed composite fading models, such as the $\kappa - \mu$/inverse gamma model, for different PLC-WLC propagation environments are clear. Therefore, it can be concluded, as indicated by the obtained results, that the amount of shadowing increases as more branches or discontinuities (non-idealities) are added to the PLC portion of the hybrid PLC-WLC channel, which results in increased multipath propagation behavior, because the instances of DM-to-CM conversions in the PLC channel increases instances of signal emissions thereby creating new signal components and propagation paths in the WLC portion of the hybrid PLC-WLC channel. This results in increased random mean power fluctuations in the received signal, which means increased signal shadowing, and consequently increased composite fading behavior of the hybrid PLC-WLC channel. The comprehensive results presented in this paper are important for real world narrowband PLC-WLC applications, because they can serve as a guide to practitioners and other researchers as to what is the expected time-selective fading behavior of narrowband PLC-WLC communications systems in scenarios involving relative motion between the PLC and WLC devices.

9 | Conclusion

This paper presents an in-depth investigation into composite fading behavior in hybrid PLC-WLC communication channels. Novel insights into the modelling of composite fading in the context of PLC-WLC systems, particularly under conditions involving relative motion between PLC and WLC devices, are provided. A new composite fading model, namely, the $\kappa - \mu$/GR fading model, was introduced. Analytical expressions for fundamental statistics such as the PDF, CDF, moments and MGF were derived in closed-form. Additionally, performance metrics like OP, ASEP and average channel capacity were derived for communication systems under the $\kappa - \mu$/GR channel conditions. Validation of the derived expressions for performance metrics was achieved through numerical analysis, which agreed with simulation results. The GR model, which is borrowed from statistical frameworks, was employed to describe shadowing behavior due to its mathematical tractability. Its utility and accuracy were further established through a methodical approximation of the well-established lognormal and inverse Gaussian shadowing models using the MoM estimators approach. By analyzing the relationships between the parameters of the proposed model and those of established shadowing models, it was shown that the $\kappa - \mu$/GR model closely approximates the Rice/lognormal and Rice/inverse Gaussian composite fading models.

Comprehensive measurements were conducted across various PLC-WLC propagation scenarios in indoor environments. The empirical data were fitted to the proposed model, which demonstrated an excellent fit to the measurements. For small indoor environments, rich signal scattering conditions and clustering behavior of multipath components were evident, regardless of the extent of cable branching within the PLC portion of the PLC-WLC channel. Conversely, large indoor environments exhibited pronounced scattering primarily when extensive cable branching occurred, while otherwise being dominated by strong LOS signal components under most of the propagation scenarios.

The performance of the proposed composite fading model was further validated using KL divergence tests, benchmarking it against other existing composite fading models. Results highlighted the prevalence of measurable multiplicative shadowing in several PLC-WLC propagation scenarios within both small-indoor and large-indoor environments. In the context of PLC-WLC systems, where no direct LOS signal path exists between a PLC transmitter and a WLC receiver, the powerline effectively acts as an antenna element. This allows signal emissions across diverse locations with varying signal strengths. The findings in this study indicate that the key determinant for distinguishing LOS shadowing from multiplicative shadowing models is the presence of dominant signal components and the observed power disparity between dominant and scattered components. As such, LOS shadowing and multiplicative shadowing composite fading models can both be applied to characterize time-selective fading across distinct propagation conditions. As the results suggest, increased branching, discontinuities and terminations within the PLC channel in a PLC-WLC propagation environment lead to greater shadowing and multipath fading, resulting in increased composite fading.

Acknowledgments

The authors have nothing to report.

Conflicts of Interest

The authors declare no conflicts of interest.

Data Availability Statement

The datasets used and/or analyzed during the current study are available from the corresponding author on reasonable request.

References

1. W. Braun and U. Dersch, "A Physical Mobile Radio Channel Model," *IEEE Transactions on Vehicular Technology* 40, no. 2 (1991): 472–482.

2. H. Suzuki, "A Statistical Model for Urban Radio Propagation," *IEEE Transactions on Communications* 25, no. 7 (1977): 673–679.

3. C. Loo, "A Statistical Model for a Land Mobile Satellite Link," *IEEE Transactions on Vehicular Technology* 34, no. 3 (1985): 122–127.

4. A. Abdi and M. Kaveh, "K Distribution: An Appropriate Substitute for Rayleigh-Lognormal Distribution in Fading Shadowing Wireless Channels," *IEE Electronics Letters* 34, no. 9 (1998): 851–852.

5. I. Kostic, "Analytical Approach to Performance Analysis for Channel Subject to Shadowing and Fading," *IEE Proceedings-Communications* 152, no. 6 (2005): 821–827.

6. Karmeshu and R. Agrawal, "On Efficacy of Rayleigh-Inverse Gaussian Distribution Over k-Distribution for Wireless Fading Channels. Wireless Communications Mobile," *Computing* 7, no. 1 (2007): 1–7.

7. A. Laourine, M. S. Alouini, S. Affes, and A. Stephenne, "On the Performance Analysis of Composite Multipath/Shadowing Channels Using the g-Distribution," *IEEE Transactions on Communications* 57, no. 4 (2009): 1162–1170.

8. M. D. Yacoub, "The κ-μ Distribution and the η-μ Distribution," *IEEE Antennas and Propagation Magazine* 49, no. 1 (2007): 68–81.

9. M. D. Yacoub, "The α-μ Distribution: A Physical Fading Model for the Stacy Distribution," *IEEE Transactions on Vehicular Technology* 56, no. 1 (2007): 27–34.

10. S. L. Cotton, "A Statistical Model for Shadowed Body-Centric Communications Channels: Theory and Validation," *IEEE Transactions on Antennas and Propagation* 62, no. 3 (2014): 1416–1424.

11. P. C. Sofotasios, T. A. Tsiftsis, K. H. Van, S. Freear, L. R. Wilhelmsson, and M. Valkama, "The κ μ /ig Composite Statistical Distribution in RF and FSO Wireless Channels," in *IEEE Vehicular Technology Conference* (IEEE, 2013), 1–5.

12. P. C. Sofotasios, T. A. Tsiftsis, M. Ghogho, L. R. Wilhelmsson, and M. Valkama, "The η μ /ig Distribution: A Novel Physical Multipath/Shadowing Fading Model," in *IEEE International Conference on Communications* (IEEE, 2013), 5715–5719.

13. P. C. Sofotasios and S. Freear, "On the κ-μ /Gamma Composite Distribution: A Generalized Multipath/Shadowing Fading Model," in *IEEE International Microwave and Optoelectronics Conference* (IEEE, 2011), 390–394.

14. S. K. Yoo, S. L. Cotton, P. C. Sofotasios, and S. Freear, "Shadowed Fading in Indoor Off-Body Communication Channels: A Statistical Characterization Using the κ μ /Gamma Composite Fading Model," *IEEE Transactions on Wireless Communications* 15, no. 8 (2016): 5231–5244.

15. P. C. Sofotasios and S. Freear, "The η μ /Gamma Composite Fading Model," in *IEEE International Conference on Wireless Information Technology and Systems* (IEEE, 2010), 1–4.

16. J. Zhang, M. Matthaiou, Z. Tan, and H. Wang, "Performance Analysis of Digital Communication Systems Over Composite $\eta - \mu$ /Gamma Fading Channels," *IEEE Transactions on Vehicular Technology* 61, no. 7 (2012): 3114–3124.

17. S. K. Yoo, N. Simmons, S. L. Cotton, et al., "The κ-μ/ Inverse Gamma and η-μ /Inverse Gamma Composite Fading Models: Fundamental Statistics and Empirical Validation," *IEEE Transactions on Communications* 69, no. 8 (2021): 5514–5530.

18. S. L. Cotton, "Human Body Shadowing in Cellular Device-to-Device Communications: Channel Modeling Using the Shadowed κ-μ Fading Model," *IEEE Journal on Selected Areas in Communications* 33, no. 1 (2015): 111–119.

19. P. Ramrez-Espinosa and F. J. Lpez-Martnez, "Composite Fading Models Based on Inverse Gamma Shadowing: Theory and Validation," *IEEE Transactions on Wireless Communications* 20, no. 8 (2021): 5034–5045.

20. N. Simmons, C. R. N. D. Silva, S. L. Cotton, P. C. Sofotasios, S. K. Yoo, and M. D. Yacoub, "On Shadowing the κ μ Fading Model," *IEEE Access* 8 (2020): 120,513–120,536.

21. H. Hashemi, "The Indoor Radio Propagation Channel," *Proceedings of the IEEE* 81, no. 7 (1993): 943–968.

22. I. Snchez and F. J. Lpez-Martnez, "The Lomax Distribution for Wireless Channel Modeling: Theory and Applications," *IEEE Open Journal of Vehicular Technology* 5 (2024): 162–171.

23. I. Snchez and F. J. Lpez-Martnez, "A Formulation of the Log-Logistic Distribution for Fading Channel Modeling," *Electronics* 11, no. 15 (2022).

24. P. Favre, C. Candolfi, M. Schneider, M. Rubinstein, P. Krahenbuehl, and A. Vukicevic, "Common Mode Current and Radiations Mechanisms in plc Networks," in *IEEE International Symposium on Power Line Communications and Its Applications* (IEEE, 2007), 348–354.

25. C. Kikkert, *MATLAB for Engineers - Applications in Control, Electrical Engineering, IT and Robotics*, 1st ed. (IntechOpen, 2011).

26. A. Mescco, P. Pagani, M. Ney, and A. Zeddam, "Radiation Mitigation for Power Line Communications Using Time Reversal," *Journal of Electrical and Computer Engineering* 2013, no. 1 (2013): 402–514.

27. D. Righini, F. Passerini, and A. M. Tonello, "Modeling Transmission and Radiation Effects When Exploiting Power Line Networks for Communication," *IEEE Transactions on Electromagnetic Compatibility* 60, no. 1 (2018): 59–67.

28. T. Oliveira, F. Andrade, A. Picorone, H. Latchman, S. Netto, and M. Ribeiro, "Statistical Characterization of κ-μ Shadowed Fading," *Journal of Computer Information Systems* 31, no. 1 (2016): 224–235.

29. T.d. A. Nogueira, G. R. Colen, V. Fernandes, and M. Ribeiro, "Statistical Modeling of Magnitudes of Brazilian In-Home PLC and Hybrid PLC-Wireless Channels," *Physical Communication* 39 (2020): 101,014.

30. F. Igboamalu, A. Ndjiongue, A. deBeer, and H. C. Ferreira, "Contact-Less PLC: Channel Analysis and Measurements Campaign," *Telecommunication Systems* 77 (2021): 389–398.

31. K. Mokise and H. Myburgh, "Composite Fading in Powerline-Wireless Communication Channels: Characterisation of Small-Scale and Large-Scale Fading". In: IEEE International Conference on Communications, Control, and Computing Technologies for Smart Grids, pp. 187–192, (2024).

32. D. Hockanson, J. Dreniak, T. Hubing, T. van Doren, F. Sha, and C. W. Lam, "Quantifying EMI Resulting From Finite-Impedance Reference Planes," *IEEE Transactions on Electromagnetic Compatibility* 39, no. 4 (1997): 286–297.

33. D. Hockanson, J. Drewniak, T. Hubing, T. Van, F. Sha, and M. Wilhelm, "Investigation of Fundamental EMI Source Mechanisms Driving Common-Mode Radiation From Printed Circuit Boards With Attached Cables," *IEEE Transactions on Electromagnetic Compatibility* 38, no. 4 (1996): 557–566.

34. J. F. Paris, "Statistical Characterization of κ-μ Shadowed Fading," *IEEE Transactions on Vehicular Technology* 63 (2013): 518–526.

35. A. Alzaatreh, C. Lee, and F. Famoye, "A New Method for Generating Families of Continuous Distributions," *Metron* 71, no. 1 (2013): 63–79.

36. E. E. E. Akarawak, I. A. Adeleke, and R. O. Okafor, "The Gamma-Rayleigh Distribution and Applications to Survival Data," *Nigerian Journal of Basic and Applied Sciences* 25, no. 2 (2017): 130–142.

37. A. P. Prudnikov, Y. A. Brychkov, and O. I. Marichev, *Integrals and Series - Special Functions*, vol. 2 (Gordon and Breach Science Publishers, 1986).

38. A. Erdlyi, W. Magnus, F. Oberhettinger, and F. G. Tricomi, *Tables of Integral Transforms*, vol. 1 (McGraw-Hill Book Company, Inc, 1954).

39. I. S. Gradshteyn, I. M. Ryzhik, A. Jeffrey, and D. Zwillinger, *Table of Integrals, Series, Products*, 7th ed. (Academic, 2007).

40. T. Eltoft, "The Rician Inverse Gaussian Distribution: A New Model for Non-Rayleigh Signal Amplitude Statistics," *IEEE Transactions on Image Processing* 14, no. 11 (2005): 1722–1735.

41. A. Abdi and M. Kaveh, "Performance Comparison of Three Different Estimators for the Nakagami m Parameter Using Monte Carlo Simulation," *IEEE Communications Letters* 4, no. 4 (2000): 119–121.

42. J. Cheng and N. Beaulieu, "Generalized Moment Estimators for the Nakagami Fading Parameter," *IEEE Communications Letters* 6, no. 4 (2002): 144–146.

43. M. Zimmermann and K. Dostert, "Analysis and Modeling of Impulsive Noise in Broad-Band Powerline Communications," *IEEE Transactions on Electromagnetic Compatibility* 44, no. 1 (2002): 249–258.

44. A. P. Prudnikov, Y. A. Brychkov, and O. I. Marichev, *Integrals and Series - Direct Laplace Transform*, vol. 4 (Gordon and Breach Science Publishers, 1992).

45. A. P. Prudnikov, Y. A. Brychkov, and O. I. Marichev, *Integrals and Series - More Special Functions*, vol. 3 (Gordon and Breach Science Publishers, 1992).

46. Y. A. Brychkov and N. Saad, "Some Formulas for the Appell Function F_1 (*a, b, b; c, w, z*)," *Integral Transforms and Special Functions* 23, no. 11 (2012): 793–802.

47. P. Njemcevic, A. Lipovac, and V. Lipovac, "Recommendations for Shadow Fading Estimation From Received Composite Signal Samples," *Wireless Networks* 26, no. 2 (2020): 1057–1067.

48. A. Abdi, W. Lau, M. S. Alouini, and M. Kaveh, "A New Simple Model for Land Mobile Satellite Channels: First- and Second-Order Statistics," *IEEE Transactions on Wireless Communications* 2, no. 3 (2003): 519–528.